Carbohydrate Polymers 91 (2013) 711–717

Contents lists available at SciVerse ScienceDirect

Carbohydrate Polymers

journal homepage: www.elsevier.com/locate/carbpol

Thermal and mechanical properties of bio-nanocomposites reinforced by *Luffa cylindrica* cellulose nanocrystals

Gilberto Siqueira [a], Julien Bras [a], Nadège Follain [b], Sabrina Belbekhouche [b], Stéphane Marais [b], Alain Dufresne [a,*]

[a] The International School of Paper, Print Media and Biomaterials (Pagora), Grenoble Institute of Technology, BP 65, 38402 Saint Martin d'Hères Cedex, France
[b] Université de Rouen, Laboratoire «Polymères, Biopolymères, Surfaces», UMR 6270 CNRS & FR3038 INC3M, 76821 Mont-Saint-Aignan Cedex, France

ARTICLE INFO

Article history:
Received 14 May 2012
Received in revised form 17 August 2012
Accepted 18 August 2012
Available online 24 August 2012

Keywords:
Cellulose nanocrystals
Luffa cylindrica
Nanocomposites
Surface chemical grafting
Mechanical properties

ABSTRACT

Cellulose nanocrystals have been prepared by acid hydrolysis of *Luffa cylindrica* fibers. The acid-resistant residue consisted of rod-like nanoparticles with an average length an diameter around 242 and 5.2 nm, respectively (aspect ratio around 46). These cellulose nanocrystals have been used as a reinforcing phase for the processing of bio-nanocomposites using polycaprolactone (PCL) as matrix. To promote interfacial filler/matrix interactions the surface of cellulose nanocrystals was chemically modified with n-octadecyl isocyanate ($C_{18}H_{37}NCO$). Evidence of the grafting was supported by infrared spectroscopy and elemental analysis. X-ray diffraction analysis was used to confirm the integrity of cellulose nanocrystals after chemical modification. Both unmodified and chemically modified nanocrystals were used to prepare nanocomposites. The thermal properties of these materials were determined from differential scanning calorimetry and their mechanical behavior was evaluated in both the linear and non-linear range.

1. Introduction

Materials, together with energy and information, are regarded as the pillar industries in the world economy of twenty-first century. An increasing demand emerges for biodegradable materials and products made from renewable resources. Moreover, replacement of traditional microcomposites by nanocomposite materials has grown rapidly during the last two decades to overcome the limitations of the micrometer-scale, designing new materials and structures with unprecedented flexibility, improved physical properties and significant industrial impact.

All these requirements are fulfilled by nano-scaled cellulose. It is the most abundant polymer on earth, it is biodegradable and its structural hierarchy can be used to prepare high strength nanoparticles. An abundant and exponentially increasing literature is devoted to cellulose nanoparticles obtained either (i) by a disintegration shearing action to obtain microfibrillated cellulose (Siró and Plackett, 2010) or (ii) by a chemical acid hydrolysis treatment to obtain cellulose nanocrystals or whiskers (Azizi Samir, Alloin, & Dufresne, 2005; Habibi, Lucia, & Rojas, 2010; Moon, Martini, Nairn, Simonsen, & Youngblood, 2011). Several sources of cellulose have been used to prepare such cellulosic nanoparticles. Generally, the elongated rod-like cellulose nanocrystals consist of high-purity single cellulose nanocrystals formed from a variety of cellulose fiber sources under controlled conditions whose dimensions depend on the nature of cellulose source as well as the hydrolysis conditions. Their diameter and length typically range from 5 to 10 nm and from 100 to 500 nm, respectively.

Fibers extracted from a tropical plant named *Luffa cylindrica*, belonging to the family of *Cucurbitacea*, has been recently studied as a new potential source of microfibrillated cellulose and cellulose nanocrystals (Siqueira, Bras, & Dufresne, 2010a) able to impact the properties of bio-nanocomposites. In fact, the *L. cylindrica* cellulose has been investigated in the field of polymer composites owing to its high cellulose content and its density around 0.82 and 0.92 g cm^{-3} (Satyanarayana, Guilmaraes, & Wypych, 2007) lower than the one of some common natural fibers such as sisal (1.26 g cm^{-3}), hemp (1.48 g cm^{-3}) or ramie (1.5 g cm^{-3}) and cotton (1.51 g cm^{-3}) (Siqueira et al., 2010a). However, to be efficiently used as a reinforcing phase in a polymeric matrix material, the surface of the cellulosic filler usually needs to be compatibilized to reduce its inherent hydrophilic character and improve its dispersability in the continuous phase which is generally hydrophobic. Several possibilities have already been described and the positive impact of such surface treatment has been confirmed with PCL-nanocellulose composites (Siqueira, Bras, & Dufresne, 2009). In this case, sisal based nanocellulose were used. Up to our knowledge, the influence of source of whiskers on PCL

* Corresponding author. Tel.: +33 4 76 82 69 95; fax: +33 4 76 82 33.
E-mail address: Alain.Dufresne@pagora.grenoble-inp.fr (A. Dufresne).

0144-8617/$ – see front matter © 2012 Elsevier Ltd. All rights reserved.
http://dx.doi.org/10.1016/j.carbpol.2012.08.057

nanocomposites thermal and mechanical properties has never been proposed.

Such nanocomposite materials can also have an interest regarding transport properties as very recently published on similar PCL-*L. cylindrica* whiskers composites (Follain et al., submitted for publication). In the present study, cellulose nanocrystals extracted from *L. cylindrica* fibers have been used to prepare fully biodegradable bio-nanocomposites with a polycaprolactone matrix and their thermal and mechanical properties have been analyzed and compared with other sources.

2. Experimental

2.1. Materials and processing

Native *L. cylindrica* fibers were purchased in Belo Horizonte (Minas Gerais, Brazil). Poly(caprolactone) (PCL) (Mn = 42,500 g mol^{-1}, Mw = 65,000 g mol^{-1}), sulfuric acid (≥95 wt%), and N-octadecyl isocyanate were obtained from Aldrich. Ethanol, acetone, chloroform, toluene, and dichloromethane were purchased from Chimie-Plus and used as delivered.

2.1.1. Cellulose nanocrystals

Cellulose nanocrystals were prepared from *L. cylindrica* fibers as described elsewhere (Siqueira et al., 2010a). Briefly, fibers were treated three times with 4 wt% NaOH solution at 80 °C for 2 h under mechanical stirring and bleached with a solution made by equal parts of acetate buffer, aqueous chlorite (1.7 wt% in water) and distilled water. The bleaching treatment was performed 4 times at 80 °C, under mechanical stirring, during 2 h each one. Acid hydrolysis was achieved at 50 °C with 65 wt% sulfuric acid (pre-heated), for 40 min, using mechanical stirring. Successive centrifugations were performed at 10,000 rpm and 10 °C for 10 min each step and the suspensions was dialyzed against distillated water. Homogenization was carried out using an Ultra Turax T25 homogenizer for 5 min and the suspensions was filtered in glass filter no. 1. Some drops of chloroform were added to the nanocrystal suspension that was stored at 4 °C.

2.1.2. Surface chemical modification

The surface chemical modification of *L. cylindrica* nanocrystals was performed in toluene as described elsewhere for sisal nanocrystals (Siqueira, Bras, & Dufresne, 2010b). To avoid drying of the nanocrystals that undoubtedly should lead to a strong aggregation process we used never dried cellulose. A solvent exchange procedure from water to toluene was used. For that, an aqueous suspension with the desired amount of cellulose nanocrystals (1 wt%) was solvent exchanged to acetone and then to dry toluene by several successive centrifugation and redispersion operations. Sonication was performed after each solvent exchange step to avoid aggregation.

In a three-necked round-bottomed flask, equipped with a reflux condenser, 3 g of cellulose nanocrystals in toluene and 100 mL of toluene were added. The system was kept in a nitrogen atmosphere. An excess of *n*-octadecyl isocyanate (16.9 g) was added drop by drop when the temperature of the system reached 90 °C. The temperature was then increased up to 110 °C and it was kept in this condition for 30 min. The modified nanocrystals were filtered and washed with ethanol to remove amines formed during the reaction and the isocyanate that did not react. Afterward, the modified materials were washed with ethanol and centrifuged four times at 10,000 rpm and 10 °C for 15 min each step. The final step consisted in changing the solvent of the modified nanocrystals from ethanol to dichloromethane, which was the solvent used for the film preparation.

2.1.3. Preparation of nanocomposite films

Polycaprolactone (PCL, Mn = 42,500 g mol^{-1}) was first dissolved in dichloromethane at room temperature for 20 h (0.036 g L^{-1}). Different amounts of *L. cylindrica* nanocrystals (3, 6, 9 and 12 wt% calculated on the dry basis) were used to prepare nanocomposites. The corresponding nanocrystal content in dichloromethane suspensions was magnetically stirred for 6 h with the PCL solution. The suspensions were sonicated for 2 min before casting in Teflon molds and solvent evaporation was performed at room temperature. The thickness of nanocomposites was approximately 350 ± 50 μm from the average value of 13 measurements per film.

The designation of nanocomposites is reported as follows: PCL/*X* wt% ULW nanocomposite and PCL/*X* wt% MLW nanocomposite, with X being the weight content of nanocrystals within the nanocomposite film, ULW and MLW designing unmodified and modified *L. cylindrica* nanocrystals, respectively.

2.2. Characterizations

2.2.1. Morphological analyses

Transmission electron microscopy (TEM) observations were performed with a Philips CM200 transmission electron microscope using an acceleration voltage of 80 kV. A drop of diluted suspension of *L. cylindrica* nanocrystals was deposited on a carbon-coated grid. The samples were stained with a 2 wt% solution of uranyl acetate.

Elemental analysis was carried out at the Laboratoire Central d'Analyses de Vernaison, France (CNRS). The carbon, oxygen, hydrogen and nitrogen contents for unmodified and modified *L. cylindrica* nanoparticles were measured independently. The results from elemental analysis were used to determine the degree of substitution (DS, number of grafted hydroxyl function per anhydroglucose unit (AGU)) according to Eq. (1):

$$DS = \frac{72.07 - C \times 162.14}{281.48 \times C - 216.20} \quad (1)$$

where *C* is the relative carbon content in the sample and 72.07, 162.14, 281.48, 216.20 correspond to the molecular weight of the anhydroglucose unit, mass of anhydroglucose unit, mass of n-octadecyl isocyanate residue and carbon mass of the n-octadecyl isocyanate residue, respectively.

The obtained values were averaged over two measurements and the standard deviation ranged between 0.10 and 0.30. The precision of the measurement was considered to be 0.3% for C and H atoms, and 0.5% for O atoms. They have been corrected assuming unmodified samples as pure cellulose and samples made during the same analysis series.

Infrared spectroscopy (FTIR) was used to evidence the chemical grafting of cellulose nanocrystals. FTIR spectrograms were recorded by directly depositing the dried powder of nanoparticles on the surface of the crystal. FTIR analysis was performed with a Mattson 5000 spectrometer, equipped with single reflection HATR and a ZnSe crystal using a resolution of 4 cm^{-1} and with a total of 64 scans.

X-ray diffraction analysis were recorded with a Panalytical X' Pert Pro MPD-Ray diffractometer with Ni-filtered Cu Kα radiation (λ = 1.54 Å) generated at a voltage of 45 kV and current of 40 mA. The 2θ diffraction diagrams were determined between 5° and 60°. The crystallinity index was calculated using the Buschle–Diller and Zeronian equation (Eq. (2)) (Buschle-Diller & Zeronian, 1992):

$$I_c = \frac{1 - I_1}{I_2} \quad (2)$$

where I_1 is the intensity at the minimum (2θ = 18°) and I_2 is the intensity associated with the crystalline region of cellulose (2θ = 22.5°).

2.2.2. Tensile tests

Tensile tests were performed under ambient conditions (25 °C) on a RSA3 (TA instrument, USA) equipment with a 100 N load cell, and with a cross head speed of 10 mm min^{-1}. The samples were prepared by cutting strips of the films 20 mm long and the distance between jaws was 10 mm, whereas the width and the thickness of the samples were measured before each test. The stress–strain curves were plotted and the tensile modulus was deduced from the low strain region. At least five specimens were tested to characterize each set of PCL based nanocomposite and the mean values were also reported for ultimate mechanical properties, i.e. nominal strain at break and nominal strength.

2.2.3. Thermal analysis

Differential scanning calorimetry (DSC) experiments were performed on PCL based nanocomposites with a DSC Q100 differential calorimeter (TA instruments, USA) fitted with a manual liquid nitrogen cooling system. The samples with weight comprised between 6 mg and 10 mg were placed in hermetically closed DSC devices under nitrogen atmosphere to minimize the oxidative degradation. The heating and cooling steps were carried out from −100 °C to 100 °C and from 100 °C to −100 °C, respectively, at a rate of 10 °C min^{-1}. The glass transition (T_g) and melting (T_m) temperatures were taken as the specific heat increment and peak temperature of the melting endotherm, respectively, while the heat of fusion was calculated from the area of the peaks. The degree of crystallinity (χ_C) was determined from DSC thermograms using the relationship:

$$\chi_C = \frac{\Delta H_m}{w \cdot \Delta H_m^\circ} \quad (3)$$

where $\Delta H_m^\circ = 157$ J g^{-1} was taken for 100% crystalline PCL and w is the weight fraction of PCL matrix in the nanocomposite.

2.2.4. Dynamic mechanical analysis

Dynamical mechanical analysis (DMA) of the nanocomposite films was carried out using a RSA3 (TA Instruments, USA) equipment working in tensile mode. The measurements were performed at a constant frequency of 1 Hz, strain amplitude of 0.05%, in the temperature range from −100 °C to 100 °C, a heating rate of 5 °C min^{-1} and a distance between jaws of 10 mm. The width of the samples varied from 3 to 5 mm, which were measured before each analysis. Two samples were used to characterize each nanocomposite.

3. Results and discussion

3.1. Morphological analyses of L. cylindrica nanocrystals

The geometrical characteristics of *L. cylindrica* nanocrystals have been investigated from TEM observation by using digital image analysis (ImageJ). Fig. 1 shows the TEM micrograph of well-dispersed elongated rod-like *L. cylindrica* nanoparticles. The *L. cylindrica* nanocrystals exhibit an average diameter of 5.2 ± 1.3 nm and length of 242 ± 86 nm determined from a minimum of 50 measurements, giving rise to an aspect ratio around 46.5. This value is typically in the aspect ratio range of cellulose nanocrystals regardless the cellulose source and the growth conditions (Dufresne, 2008).

It is found to be higher than the one of nanocrystals extracted from other annual plants such as ramie (L/d = 12 (de Menezes, Siqueira, Curvelo, & Dufresne, 2009)), bagasse pulp (L/d = 13 (Bras et al., 2010) and cotton (L/d = 11–12 (Roohani et al., 2008)). It is similar to values reported for sisal (L/d = 43 (Siqueira et al., 2009)) allowing comparison of the 2 sources. A recent review dedicated to research into cellulose and nanocomposites reported that an efficient reinforcement effect in composite materials can be guarantied when nanofibers with an aspect ratio around 50 are incorporated into a polymer matrix compared with conventional micro-sized fibers (Eichhorn et al., 2010).

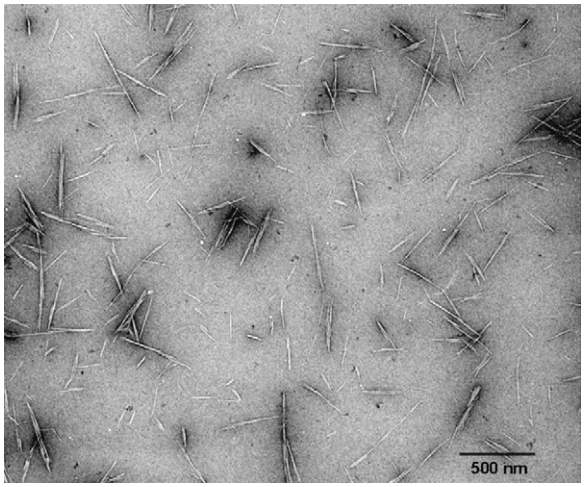

Fig. 1. Transmission electron micrograph of unmodified *Luffa cylindrica* nanocrystals.

To overcome the low interfacial compatibility between hydrophilic cellulose nanowhiskers and hydrophobic polymer, surface-chemical modification of *L. cylindrica* nanocrystals with long aliphatic chains was carried out as explained in Section 2. The successful surface-chemical grafting of *n*-octadecyl isocyanate was confirmed using FTIR spectroscopy, and quantified from elemental analysis.

Well-known FTIR bands specific to cellulose are present in FTIR spectrum shown in Fig. 2 such as hydroxyl groups at 3496 cm^{-1} and —CH band located around 2800–2900 cm^{-1}.

After surface chemical grafting, an increase of the FTIR bands at 2868 and at 2970 cm^{-1} is observed and attributed to alkyl chains corresponding to asymmetric and symmetric —CH_2— stretching band from the long chains of grafting agent. New signals are also obtained ensuring the grafting of $C_{18}H_{37}NCO$ isocyanate agent by urethane bonding formations at 1732 cm^{-1} (peak) and at 1537 cm^{-1} (shoulder) corresponding to the carbonyl stretching

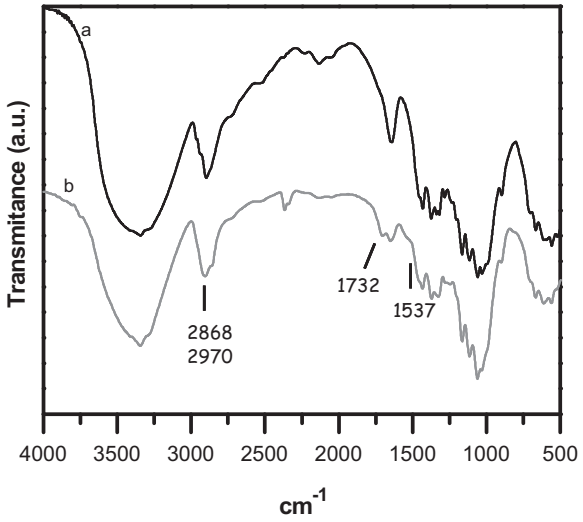

Fig. 2. FTIR spectrum for (a) unmodified and (b) chemically modified *Luffa cylindrica* nanocrystals.

Table 1
Experimental and corrected elemental weight compositions for unmodified and modified *Luffa cylindrica* nanocrystals and efficiency of grafting in terms of the number of isocyanate chains grafted par AGU unit.

Samples		Experimental values				Corrected values		DS
		%C	%H	%N	%O	%C	%O	
Luffa cylindrica	ULW	41.20	6.23	<0.10	51.27	44.44	49.38	–
Nanocrystals	MLW	43.44	6.56	0.30	47.13	46.86	45.39	0.05

Note: DS corresponds to the number of chains grafted per glucose unit (AGU).
ULW: unmodified *Luffa cylindrica* nanocrystals.
MLW: modified *Luffa cylindrica* nanocrystals.

and amine bending, respectively. The signal generally attributed to the untreated isocyanate functionality located at 2270 cm^{-1} is not observed showing that no physically absorbed long-chain isocyanate is present. These observations agree well with recently published results on the surface grafting on sisal (Siqueira et al., 2010b), as well as ramie (Zoppe, Peresin, Habibi, Venditti, & Rojas, 2009) nanocrystals. Grafting of *n*-octadecyl isocyanate on *L. cylindrica* nanocrystals and proof of urethane formation is then given by FTIR characterization and strong washing of the cellulosic material is found to be effective to eliminate by-products and unreacted species.

Determination of the elemental weight compositions and degree of substitution (DS) of unmodified and chemically modified *L. cylindrica* nanocrystals are reported in Table 1. The DS value, i.e. the number of grafted hydroxyl function per anhydroglucose moiety, was determined on the basis of elemental analysis (Eq. (1)). The experimental values reported in Table 1 refer to data obtained directly from elemental analysis whereas the corrected values refer to the product between the experimental value obtained for a given substrate and the ratio of the theoretical to experimental value for unmodified substrate. For chemically modified *L. cylindrica* nanoparticles, the DS value is around 0.05 meaning that 5 chains of isocyanate were grafted for each 100 AGU units of cellulose. This result agrees well with recently published data on the surface chemical modification of sisal nanocrystals (DS = 0.06) (Siqueira et al., 2010b). However, this low value is interpreted as being at the limit of the elemental analysis technique precision (Peydecastaing, Vaca-Garcia, & Borredon, 2009). Nevertheless, a low amount of grafted long-chain agent is generally sufficient to strongly modify the surface energy of cellulose substrate (Siqueira et al., 2010b). This low value suggests that the reaction was mainly limited to accessible hydroxyl groups present at the surface of cellulose nanocrystals that may contain less-ordered regions (Freire, Silvestre, Neto, Belgacem, & Gandini, 2006).

X-ray diffraction measurements were performed on both unmodified and chemically modified *L. cylindrica* nanocrystals to ascertain the integrity of nanoparticle crystallinity. The chemically modified nanocrystals display the typical XRD pattern of cellulose I as shown in Fig. 3 with main diffraction signals at $2\theta = 14.8$, 16.8, 23.3 and 34.9° assigned to (1 0 1), (1 0 $\bar{1}$), (0 0 2) and (0 4 0) diffraction planes, respectively (Sassi, Tekely, & Chanzy, 2000; Bras et al., 2010). No significant alteration of the XRD cellulose pattern can be noted suggesting that the reaction occurred predominantly on the surface without affecting in a great extent the internal structure of the material.

Upon long-chain surface chemical modification, a new ill-defined peak (located by an arrow in Fig. 3) appears around 21° and is ascribed to the presence of grafted aliphatic chains. This result is in agreement with the few experiments reported in the literature on the grafting of long-chain polymers on nano-sized substrates. A similar peak for PCL- (Habibi & Dufresne, 2008) and organic acid chloride aliphatic chains-grafted (de Menezes et al., 2009) cellulose nanocrystals was reported. It can be noted that the strong diffraction peak due to cellulose I occurring in the same diffraction angle range has given rise to this less defined diffraction peak.

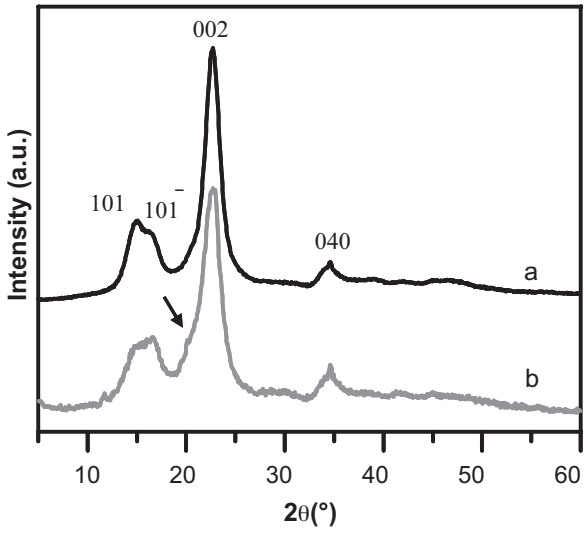

Fig. 3. X-ray diffraction patterns for (a) unmodified and (b) chemically modified *Luffa cylindrica* nanocrystals.

On the basis of Buschle–Diller and Zeronian method (Eq. (2)), the crystallinity index (I_c) calculated from the intensity of the contribution from crystalline and amorphous regions to the XRD patterns is reported in Table 2. The I_c value is of the same order than values reported for sisal (Siqueira et al., 2010b), ramie (de Menezes et al., 2009) and sugar cane bagasse nanocrystals (Bras et al., 2010). This high value depends on the preparation conditions of nanocrystals which involved an acid hydrolysis treatment with H_2SO_4 that removes cellulosic amorphous domains. The amorphous regions surrounding and embedding cellulose microfibrils were then disrupted while leaving the microcrystalline segments intact. No significant changes of the I_c value can be noted after surface-chemical modification. However, a slight decrease is observed and could be interpreted as the introduction of a slight disorder in the outmost of cellulose nanocrystals with the grafted long-chain isocyanate. Upon surface-chemical modification, the highly crystalline regions from the surface of crystalline particles can be partially converted into poorly ordered crystalline regions.

Table 2
Crystallinity index determined from X-ray diffraction experiments for *Luffa cylindrica* nanocrystals.

Luffa cylindrica nanocrystals	Crystallinity index (%)
Unmodified – ULW	96.5
Modified – MLW	93.8

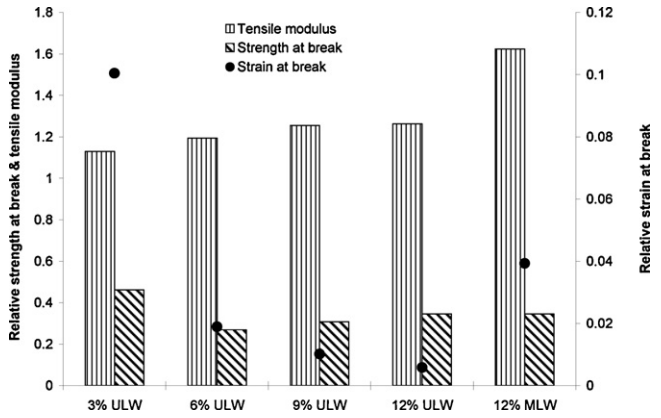

Fig. 4. Relative mechanical properties for PCL based nanocomposites reinforced with unmodified and chemically modified *Luffa cylindrica* nanocrystals.

3.2. Thermal and mechanical behavior of PCL based nanocomposites

3.2.1. Non-linear mechanical behavior

The non-linear mechanical behavior of PCL based nanocomposites was characterized by tensile tests performed at room temperature. The tensile modulus, strength and strain at break determined from typical stress–strain curves were determined for the neat PCL matrix and PCL based nanocomposites. The average relative mechanical properties are plotted in Fig. 4, for which the accuracy was found to be 10%. The relative data were calculated from the ratio of a given property divided by the one of the neat matrix.

It is worth noting that the PCL film presented a ductile behavior at room temperature and displayed a low elastic modulus that prevents its use for applications where high rigidity is required. The PCL based nanocomposites containing unmodified cellulose nanocrystals clearly displayed a slight increase in tensile modulus and a reduced strain at break which are typical results for the reinforcement of polymer matrix. This could result from the high aspect ratio of *L. cylindrica* nanocrystals. However, the enhanced rigidity observed for nanocomposites can also be linked, at least partially, to the increased degree of crystallinity of the matrix.

The decrease observed for the strength and strain at break is an indication of the brittleness induced when increasing the nanofiller content. The brittleness of these nanocomposites is ascribed to the creation of accentuated fragility domains (Habibi & Dufresne, 2008) as a consequence of poor compatibility between the unmodified *L. cylindrica* nanocrystals and PCL matrix. The extent of mechanical reinforcement can be limited by probable nanocrystal aggregation during the nanocomposite processing due to inter-particle interactions leading to the formation of weak points. This lack of intimate interfacial adhesion can induce several irregularly shaped microvoids inside the nanocomposite film.

The positive impact of the surface-chemical modification on the mechanical properties is clearly shown in Fig. 4. The stiffness of PCL with the increase in tensile modulus was markedly improved with the surface-chemical treatment of *L. cylindrica* nanocrystals (PCL/12 wt% MLW nanocomposite). In addition to the increase in strain at break, the strength at break is found to be maintained compared to mechanical data obtained for the nanocomposite reinforced with unmodified nanoparticles (Fig. 4). It can be estimated that the increase in the tensile modulus is attributed to the better filler/matrix adhesion allowing a higher homogeneity and the formation of hard domains resulting from chain tangling effect between surface-grafted cellulose nanocrystals and PCL matrix. The increase in strain at break is probably caused by the breaking of hydrogen bonding among cellulose nanocrystals allowing a higher extension of the material. However, the strain at break remains lower than for the neat PCL matrix. Such a phenomenon has been recently reported for surface modified sisal nanocrystals reinforced PCL film (Siqueira et al., 2009) even if it was less noticeable.

Table 3
Thermal characteristics of PCL based nanocomposites using data obtained from the DSC analysis: glass transition temperature (T_g), melting temperature (T_m) and associated with heat of fusion (ΔH_m), and degree of crystallinity (χ_C).

	T_g (°C)	T_m (°C)	ΔH_m (J g^{-1})	χ_C
PCL	−62.0	63.4	80.7	0.51
PCL/3 wt% ULW	−59.2	65.6	84.3	0.55
PCL/6 wt% ULW	−57.7	65.3	86.4	0.58
PCL/9 wt% ULW	−57.4	65.2	80.2	0.56
PCL/12 wt% ULW	−58.8	66.0	77.9	0.56
PCL/12 wt% MLW	−57.3	64.9	88.6	0.64

3.2.2. Thermal behavior

The glass transition temperature (T_g), melting temperature (T_m) and associated heat of fusion (ΔH_m), as well as degree of crystallinity (χ_c) were determined from DSC traces. Conventional and similar thermograms (not shown) were obtained for the PCL film and PCL based nanocomposites. The resulting thermal data calculated for PCL film, and PCL based nanocomposites reinforced with either unmodified or surface-chemically modified *L. cylindrica* nanocrystals are reported in Table 3.

In first insight, the *Tg* value seems to slightly increase when adding cellulose nanocrystals but no further significant modification is observed when varying the filler content. This could suggest that *L. cylindrica* nanocrystals restrict the rotational backbone motions of PCL polymer chains through the establishment of hydrogen bonding forces.

The compatibilization by surface-chemical grafting of *L. cylindrica* nanocrystals seems to induce a slightly more significant increase in T_g compared to the PCL matrix reinforced with unmodified nanoparticles (Table 3) indicating that the mobility of amorphous chains is in comparison restricted. This could be ascribed to enhanced interactions between grafted nanoparticles and PCL amorphous chains and possible entanglements. In most studies, T_g is generally not modified when increasing the nanocrystal content. Nevertheless, few authors observed a slight increase in the glass transition temperature of the host polymer when adding sisal cellulose (Garcia de Rodriguez, Thielemans, & Dufresne, 2006), or cotton nanocrystals (Choi & Simonsen, 2006). However, the T_g value can be also affected by the crystallinity of PCL.

The melting point was found to slightly increase from 63 °C to 65–66 °C when adding either unmodified or chemically modified *L. cylindrica* nanocrystals (Table 3). However, the nanofiller content did not seem to impact this value. The size of crystalline domains of PCL can therefore be estimated to globally remain identical. This result is consistent with previously published data for PCL reinforced with chitin nanocrystals extracted from *Riftia* tubes (Morin & Dufresne, 2002) and POE-based materials filled with tunicin nanocrystals (Azizi Samir, Alloin, Sanchez, & Dufresne, 2004). The growth of PCL crystalline domains is therefore not restricted by the presence of nanocrystals regardless its surface chemistry. This might be correlated to the low grafting reaction mentioned above.

The degree of crystallinity (χ_c) of the PCL matrix increases from 0.51 to 0.55–0.58 when adding unmodified *L. cylindrica* nanocrystals (Table 3). It seems that the nanofiller first led to an increase of χ_c followed by a progressive decrease for higher nanofiller content. Similar observations were reported for POE based nanocomposites reinforced with tunicin nanocrystals (Azizi Samir et al., 2004) and PCL reinforced with ramie nanocrystals (Habibi & Dufresne, 2008). The former effect can be ascribed to a nucleating effect of crystalline

nanofillers improving the ability of PCL polymer to crystallize and enhancing its crystallization rate. It was shown that the crystallization of PCL/nanoclay composites is governed by two phenomena corresponding to the diffusion and nucleation effects in the presence of nanoclay (Jimenez, Ogata, Kawai, & Ogihara, 1997). The authors put forward that the nucleation effect is generally observed for low nanofiller amount whereas the motion of polymer segments is hindered for higher nanofiller amount. In addition, some authors have pointed out the occurrence of a transcrystallization phenomenon corresponding to a preferential crystallization of the matrix amorphous chains at the surface of nanocrystals during the preparation process (Angellier, Molina-Boisseau, Dole, & Dufresne, 2006; Dufresne, Kellerhals, & Witholt, 1999).

This increase in crystallinity can explain, at least partially, the improvement of the stiffness of PCL/nanocrystal nanocomposites observed from tensile tests. At higher loading level, an inverse dependence with nanocrystal addition is observed implying a limitation in the increase of nanocomposite stiffness. This could be interpreted as a competition between the former phenomenon corresponding to a nucleation effect and the increase in viscosity of organic medium during the nanocomposite preparation by solvent-casting technique.

The surface-chemically modified nanocrystals present the highest nucleating effect since a significant increase of the degree of crystallinity from 0.51 to 0.64 is reported when adding 12 wt% within the PCL matrix. It could be related to an easier crystallization of PCL chains when grafted moieties interact with the matrix

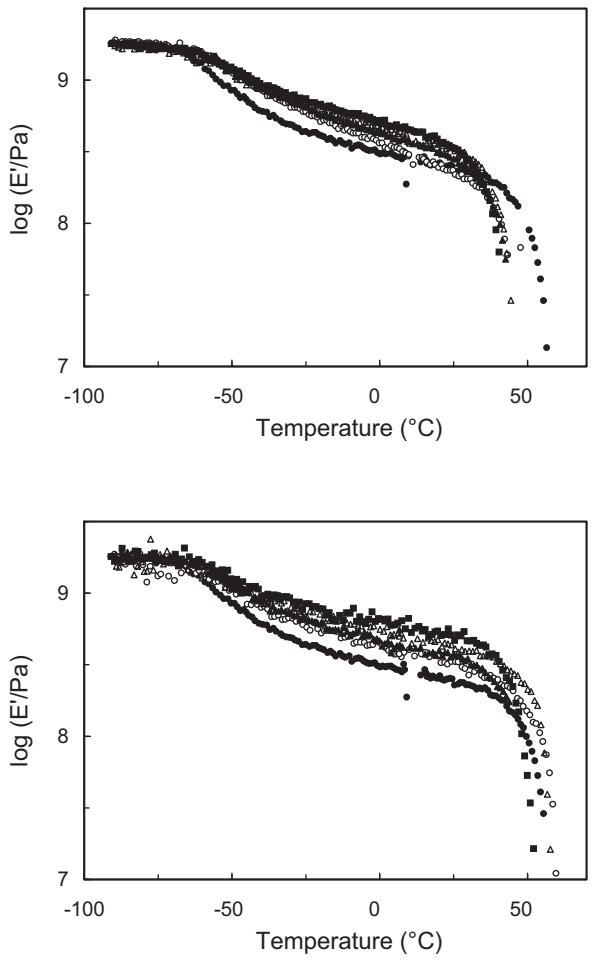

Fig. 5. Evolution of the logarithm of the storage tensile modulus as a function of temperature for the neat PCL matrix (●) and related nanocomposite films reinforced with 3 (○), 6 (▲), 9 (△), and 12 wt% (■) unmodified (A) and chemically modified (B) *Luffa cylindrica* cellulose nanocrystals.

provoking the increase in crystallinity. A higher anchoring effect of modified nanocrystals seems to be obtained probably due to the improvement in the compatibility between both material components. A similar phenomenon was suggested for topochemically silylated bacterial cellulose nanocrystals within a cellulose acetate butyrate matrix which helped to nucleate the crystallization process (Grunert & Winter, 2002). This nucleating effect of nanocrystals seems to be driven by surface chemical considerations. We recently reported a drastically acceleration of the crystallization kinetics of PCL for sisal nanocrystals based nanocomposites (Siqueira et al., 2011).

3.2.3. Linear mechanical behavior

Fig. 5 shows the evolution of the storage tensile modulus as a function of temperature for PCL based nanocomposites reinforced with unmodified (panel A) and chemically modified (panel B) *L. cylindrica* nanocrystals. The dynamic mechanical behavior of the neat PCL matrix (filled circles) is typical of a semicrystalline polymer. At lower temperatures, the modulus is of the order of few GPa because of the co-existence of glassy amorphous and crystalline domains. Around −60 °C, the modulus drops because the amorphous chains soften. It corresponds to the glass–rubber relaxation of the polymer. Up to about 50 °C, the modulus tends to stabilize but slightly decrease due to the co-existence of rubbery amorphous chains and crystalline domains that progressively melt. From this temperature a sharp irreversible modulus drop is observed because of the complete melting of the crystalline structure.

When adding unmodified cellulose nanocrystals, a slight increase of the storage modulus is observed above T_g of the matrix (Fig. 5A). This result is in agreement with non-linear tensile tests. This reinforcement effect is more pronounced when using chemically modified nanocrystals (Fig. 5B). Again, this observation agrees with non-linear tensile tests.

4. Conclusions

Sulfuric acid hydrolysis was used to prepare cellulose nanocrystals from *L. cylindrica* fibers. Ensuing rod-like nanoparticles have an average length and diameter determined from microscopic observation around 242 and 5.2 nm, respectively, giving rise to an aspect ratio around 46. Polycaprolactone (PCL) was used as matrix to prepare green nanocomposites using up to 12 wt% nanocrystals by a casting-evaporation method from dichloromethane. In order to investigate the effect of the compatibilization of the filler with matrix, the surface of cellulose nanocrystals was chemically modified with n-octadecyl isocyanate ($C_{18}H_{37}NCO$). X-ray diffraction analysis was used to confirm the integrity of cellulose nanocrystals after chemical modification. The effective grafting of long aliphatic chains was evidenced by infrared spectroscopy and elemental analysis. The degree of substitution was found to be around 0.05 but sufficient to be detectable when comparing the properties of nanocomposites prepared from unmodified and chemically modified nanocrystals. A slight increase of the glass transition temperature, melting point and degree of crystallinity of PCL was observed when adding cellulose nanocrystals. The degree of crystallinity was further increased when using modified nanoparticles. It was ascribed to a nucleating effect of nanocrystals driven by surface chemical considerations. Both non-linear and linear mechanical tests show an increase of the modulus of the nanocomposites upon addition of *L. cylindrica* nanocrystals. This effect was more marked for modified nanoparticles and probably partly due to the increased crystallinity of the PCL matrix. Moreover, chemical grafting promotes the more homogeneous dispersion of nanocrystals within the PCL as shown by the significant improvement of the elongation at break compared to unmodified nanoparticles.

Acknowledgments

The authors gratefully acknowledge ALBAN Program for the financial support (PhD fellowship of G.S.).

References

Angellier, H., Molina-Boisseau, S., Dole, P., & Dufresne, A. (2006). Thermoplastic starch–waxy maize starch nanocrystals nanocomposites. *Biomacromolecules*, *7*, 531–539.

Azizi Samir, M. A. S., Alloin, F., Sanchez, J. Y., & Dufresne, A. (2004). Cellulose nanocrystals reinforced poly(oxyethylene). *Polymer*, *45*, 4033–4157.

Azizi Samir, M. A. S., Alloin, F., & Dufresne, A. (2005). Review of recent research into cellulosic whiskers, their properties and their application in nanocomposite field. *Biomacromolecules*, *6*, 612–626.

Bras, J., Hassan, M. L., Bruzesse, C., Hassan, E. A., El-Wakil, N. A., & Dusfresne, A. (2010). Mechanical, barrier, and biodegradability properties of bagasse cellulose whiskers reinforced natural rubber nanocomposites. *Industrial Crops and Products*, *32*, 627–633.

Buschle-Diller, G., & Zeronian, S. H. (1992). Enhancing the reactivity and strength of cotton fibers. *Journal of Applied Polymer Science*, *45*, 967–979.

Choi, Y. J., & Simonsen, J. (2006). Cellulose nanocrystal-filled carboxymethyl cellulose nanocomposites. *Journal of Nanoscience and Nanotechnology*, *6*, 633–639.

de Menezes, A. J., Siqueira, G., Curvelo, A. A. S., & Dufresne, A. (2009). Extrusion and characterization of functionalized cellulose whiskers reinforced polyethylene nanocomposites. *Polymer*, *50*, 4552–4563.

Dufresne, A., Kellerhals, M. B., & Witholt, B. (1999). Transcrystallization in mcl-PHAs/cellulose whiskers composites. *Macromolecules*, *32*(22), 7396–7401.

Dufresne, A. (2008). Polysaccharide nanocrystal reinforced nanocomposites. *Canadian Journal of Chemistry*, *86*, 484–494.

Eichhorn, S. J., Dufresne, A., Aranguren, M., Marcovich, N. E., Capadona, J. R., Rowan, S. J., et al. (2010). Review: Current international research into cellulose nanofibres and nanocomposites. *Journal of Materials Science*, *45*, 1–33.

Follain, N., Belbekhouche, S., Bras, J., Siqueira, G., Marais, S., & Dufresne, A. Transport properties of bionanocomposites reinforced by Luffa cylindrica cellulose nanowhiskers, Journal of Membrane Science, submitted for publication.

Freire, C. S. R., Silvestre, A. J. D., Neto, C. P., Belgacem, M. N., & Gandini, A. (2006). Controlled heterogeneous modification of cellulose fibers with fatty acids: Effect of reaction conditions on the extent of esterification and fiber properties. *Journal of Applied Polymer Science*, *100*, 1093–1102.

Garcia de Rodriguez, N. L., Thielemans, W., & Dufresne, A. (2006). Sisal cellulose whiskers reinforced polyvinyl acetate nanocomposites. *Cellulose*, *13*, 261–270.

Grunert, M., & Winter, W. T. (2002). Nanocomposites of cellulose acetate butyrate reinforced with cellulose nanocrystals. *Journal of Polymers and the Environment*, *10*, 27–30.

Habibi, Y., & Dufresne, A. (2008). Highly filled bionanocomposites from functionalized polysaccharide nanocrystals. *Biomacromolecules*, *9*, 1974–1980.

Habibi, Y., Lucia, L. A., & Rojas, O. J. (2010). Cellulose nanocrystals: Chemistry, self-assembly, and applications. *Chemical Reviews*, *110*, 3479–3500.

Jimenez, G., Ogata, N., Kawai, H., & Ogihara, T. (1997). Structure and thermal/mechanical properties of poly (ε-caprolactone)-clay blend. *Journal of Applied Polymer Science*, *64*, 2211–2220.

Moon, R. J., Martini, A., Nairn, J., Simonsen, J., & Youngblood, J. (2011). Cellulose nanomaterials review: Structure, properties and nanocomposites. *Chemical Society Reviews*, *40*, 3941–3994.

Morin, A., & Dufresne, A. (2002). Nanocomposites of chitin whiskers from *Riftia* tubes and poly(caprolactone). *Macromolecules*, *35*, 2190–2199.

Peydecastaing, P., Vaca-Garcia, C., & Borredon, E. (2009). Accurate determination of the degree of substitution of long chain cellulose esters. *Cellulose*, *16*, 289–297.

Roohani, M., Habibi, Y., Belgacem, N. M., Ghanbar, E., Karimi, A. N., & Dufresne, A. (2008). Cellulose whiskers reinforced polyvinyl alcohol copolymers nanocomposites. *European Polymer Journal*, *44*, 2489–2498.

Sassi, J. F., Tekely, P., & Chanzy, H. (2000). Relative susceptibility of the Iα and Iβ phases of cellulose towards acetylation. *Cellulose*, *7*, 119–132.

Satyanarayana, K. G., Guilmaraes, J. L., & Wypych, F. (2007). Studies on lignocellulosic fibers of Brazil. Part I: Source, production, morphology, properties and applications. *Composites*, *38*, 1694–1709.

Siqueira, G., Bras, J., & Dufresne, A. (2009). Cellulose whiskers versus microfibrils: Influence of the nature of the nanoparticle and its surface functionalization on the thermal and mechanical properties of nanocomposites. *Biomacromolecules*, *10*, 425–432.

Siqueira, G., Bras, J., & Dufresne, A. (2010a). *Luffa cylindrica* as a lignocellulosic source of fiber, microfibrillated cellulose and cellulose nanocrystals. *BioResources*, *5*, 727–740.

Siqueira, G., Bras, J., & Dufresne, A. (2010b). New process of chemical grafting of cellulose nanoparticles with a long chain isocyanate. *Langmuir*, *26*, 402–411.

Siqueira, G., Fraschini, C., Bras, J., Dufresne, A., Prud'homme, R., & Laborie, M. P. (2011). Impact of the nature and shape of cellulosic nanoparticles on the isothermal crystallization kinetics of poly(ε-caprolactone). *European Polymer Journal*, *47*, 2216–2227.

Siró, I., & Plackett, D. (2010). Microfibrillated cellulose and new nanocomposite materials: A review. *Cellulose*, *17*, 459–494.

Zoppe, J. O., Peresin, M. S., Habibi, Y., Venditti, R. A., & Rojas, J. O. (2009). Reinforcing poly(ε-caprolactone) nanofibers with cellulose nanocrystals. *Applied Materials and Interfaces*, 1996–2004.